

A sound horizon independent measurement of H_0 from BOSS, DESI and DES Y3

Zhiyu Lu^{1,2,*}, Théo Simon^{3,†}, Vivian Poulin⁴ and Yifu Cai^{1,2}

¹*Department of Astronomy, School of Physical Sciences,*

University of Science and Technology of China, Hefei, Anhui 230026, China

²*CAS Key Laboratory for Research in Galaxies and Cosmology, School of Astronomy and Space Science,*

University of Science and Technology of China, Hefei, Anhui 230026, China

³*Laboratoire Univers et Particules de Montpellier (LUPM),*

Centre national de la recherche scientifique (CNRS) et Université de Montpellier,

Place Eugène Bataillon, 34095 Montpellier Cédex 05, France

⁴*Laboratoire univers et particules de Montpellier (LUPM),*

Centre national de la recherche scientifique (CNRS) et Université de Montpellier,

Place Eugène Bataillon, 34095 Montpellier Cédex 05, France

We present a sound horizon independent measurement of the Hubble parameter using a multiprobe large-scale structure analysis. Removing the dependency on the sound horizon with a rescaling procedure at the matter power spectrum level, we analyse the BOSS full-shape power spectrum and bispectrum (for the first time) using the effective field theory of large-scale structure up to one loop. We combine this analysis with the auto- and cross-angular power spectra from the DESI Legacy Imaging Survey DR9, the 3×2 pt analysis from DES Y3, and the CMB gravitational lensing power spectrum from *Planck* PR3. Our baseline analysis, that does not rely on supernovae data, yields $h = 0.702^{+0.022}_{-0.024}$, $\Omega_m = 0.310 \pm 0.013$, and $\sigma_8 = 0.799 \pm 0.020$, corresponding to 3 – 4% precision measurements. When adding supernovae data from Pantheon+, we obtain a 2.6% measurement of h , with $h = 0.686 \pm 0.018$. We further note that our EFTBOSS analysis indicates a slight deviation of the BAO scale parameter (at 1.8σ) from its Λ CDM value, caused by the small scales of the bispectrum. We finally use the sound horizon-free EFTBOSS analysis as a diagnosis for the presence of new physics, finding that our results are consistent with the recent hints of evolving dark energy.

I. INTRODUCTION

In recent years, several tensions between probes of the early and late universe analyzed under the Λ cold dark matter (Λ CDM) model have emerged. Among these challenges, the *Hubble tension* has attracted particular attention. This corresponds to a $\sim 5\sigma$ tension between the early-time determination of this parameter from the *Planck* collaboration, giving $H_0 = 67.36 \pm 0.54$ km/s/Mpc [1], and the local determination of this parameter from the SH0ES team [2], using a (almost) cosmological model-independent calibration of supernova distances, yielding $H_0 = 73.5 \pm 0.81$ km/s/Mpc [3]. At the same time, several CMB-independent measurements relying on the sound horizon scale r_s , which encodes the acoustic physics prior to CMB, favor constraints on H_0 that are compatible with the CMB measurements, whether they come from *Planck* [1], ACT [4] or SPT [5]. This is for instance the case of the DESI DR2 BAO measurements, combined with a Big Bang Nucleosynthesis (BBN) prior on ω_b , which gives $H_0 = 68.51 \pm 0.58$ km/s/Mpc [6]. The constraining power of these measurements is largely tied to the sound horizon r_s , motivating the development of sound horizon independent approaches. Another intriguing cosmological conundrum, is a less significant but older $\sim 2 - 3\sigma$ tension between the

weak lensing [7–9] and CMB determinations of the S_8 parameter [1, 4], which quantifies the amplitude of matter clustering (see Ref. [10] for a recent review). Even if recent reanalyses of the KiDS Legacy data [11] report a significantly reduced tension, attributed to improved photometric redshift calibration and updated analysis pipelines, the DES Y6 collaboration still report a 2.6σ tension [7]. This motivates further investigations using complementary large-scale structure (LSS) probes, even though current galaxy clustering determinations of this parameter, for instance from SDSS [12, 13] or DESI [14], are compatible with both the weak lensing and CMB. More recently, a $\sim 3\sigma$ tension has emerged on the matter abundance today Ω_m between supernovae data (from Pantheon+ [15], Union3 [16], or DES Y5 [17, 18]) and clustering data from DESI [6, 14].

In this work, we explore how a multiprobe LSS analysis can independently constrain these quantities, by exclusively considering LSS likelihoods that do not rely on the information from the sound horizon. This allows us to perform a non-trivial consistency test of the Λ CDM model by comparing sound horizon-based analyses with sound horizon-free analyses in order to isolate the impact of the sound horizon physics on the various cosmological discrepancies presented above. In addition, such an analysis is a good diagnosis of the presence of physics beyond Λ CDM in the data. For instance, Refs. [19–21] evaluate the internal consistency of SDSS/BOSS data [22], confronting sound horizon-based analyses with sound horizon-free analyses considering several types of new physics. In particular, models which alter the sound

* zhiyulu@mail.ustc.edu.cn

† theo.simon@umontpellier.fr

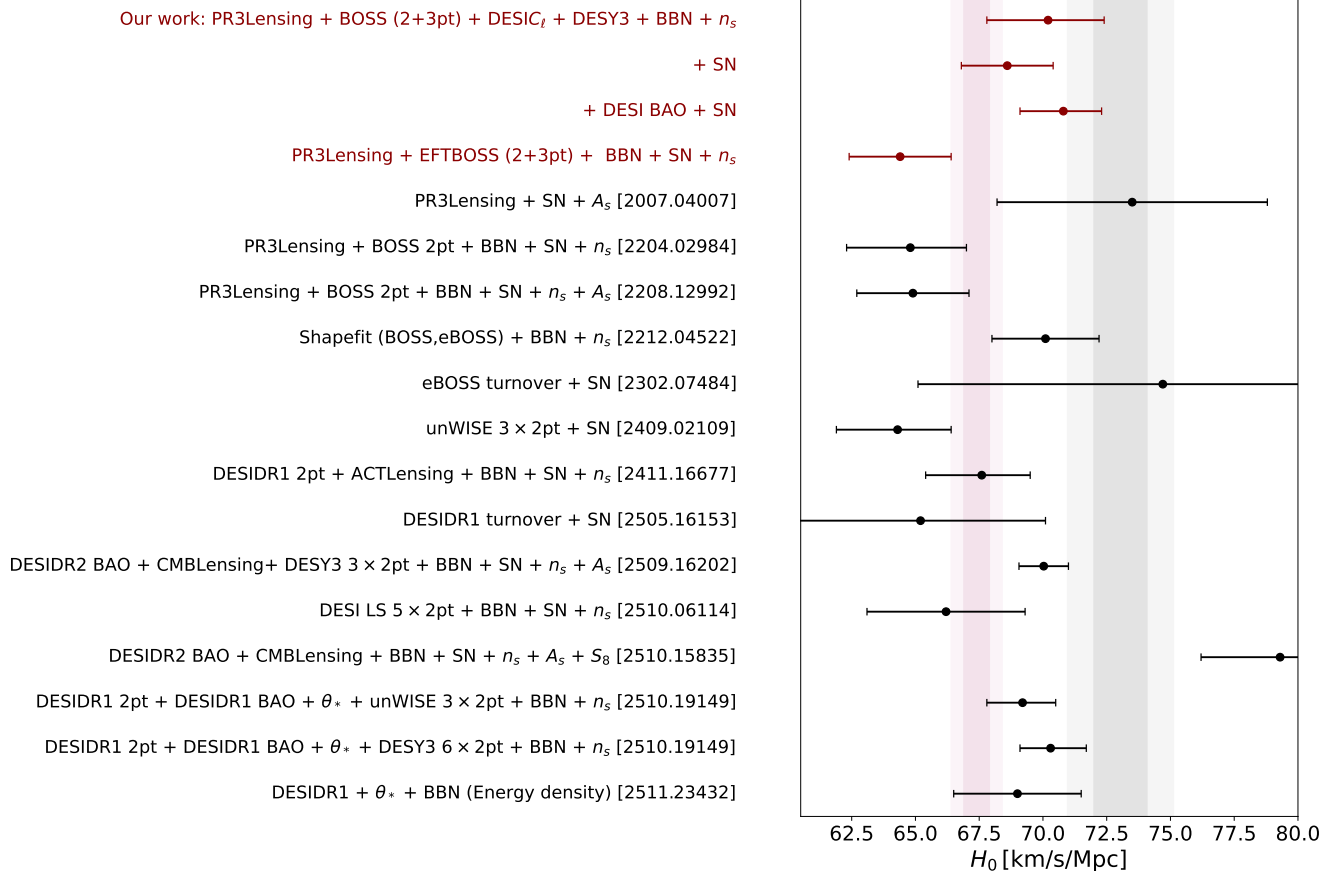


FIG. 1: Summary of recent sound horizon-free determinations of the Hubble parameter H_0 . In this plot, BAO data are always treated in a sound horizon-agnostic way, while “ n_s ”, “ A_s ” and “ S_8 ” indicate that Gaussian priors are imposed on these parameters (which are not necessarily the same for all analyses). The shaded bands denote the 1σ and 2σ regions from *Planck* [1] (in pink) and SH0ES [2] (in grey).

horizon to address the Hubble tension [23] should not be disfavoured in a sound horizon-free analysis [21] (and should be compatible with direct measurements such as the H_0 determination from SH0ES [3]).

A number of works has already derived cosmological constraints that avoid explicit dependence on the sound horizon r_s . For instance, Ref. [24] demonstrated that CMB lensing provides an approximately r_s -independent probe, since this observable is integrated along the line of sight, significantly suppressing the signal from acoustic oscillations. Using this approach, they obtained $H_0 = 73.5 \pm 5.3 \text{ km s}^{-1} \text{ Mpc}^{-1}$ from *Planck* PR3, with uncertainties large enough to be consistent with both early- and late-time measurements. Subsequent studies extended this idea to galaxy surveys. Ref. [25] measured $H_0 = 65.6^{+3.4}_{-5.5} \text{ km s}^{-1} \text{ Mpc}^{-1}$ using large-scale structure data from SDSS/BOSS by removing the prior on ω_b , which otherwise calibrates the sound horizon. Further refinements consider the wiggle-no-wiggle split procedure of the matter power spectrum [19, 21, 26, 27], which isolates the broadband shape from BAO features, improving the sound horizon-free constraint on H_0 from

large-scale structure data (together with a BBN prior on ω_b). The EFTofLSS full modeling of the broadband shape yields $H_0 = 67.1^{+2.5}_{-2.9} \text{ km s}^{-1} \text{ Mpc}^{-1}$ [20] from the BOSS galaxy power spectra. Alternatively, the *Shapefit* method models the broadband shape of the galaxy power spectrum using compressed parameters, yielding $H_0 = 70.1 \pm 2.1 \text{ km s}^{-1} \text{ Mpc}^{-1}$ for BOSS + eBOSS [28, 29], which is slightly higher than the EFTofLSS full modeling of the BOSS broadband shape. More recently, Ref. [27] performed a similar EFTofLSS-based analysis with the galaxy power spectra from DESI DR1, and found $H_0 = 67.9^{+1.9}_{-2.1} \text{ km s}^{-1} \text{ Mpc}^{-1}$, compatible with the similar BOSS analysis, with a slight deviation (at 2σ) of the BAO scale parameter from its Λ CDM value when combined with *Planck* lensing and Pantheon+, attributed to the discrepancy in Ω_m between Pantheon+ and DESI. Some other studies treat the sound horizon agnostically by taking r_s as a free parameter [30, 31]. The recent work [32] performed such an analysis using *Planck*, DESI BAO, cosmic shear and supernovae data, finding a mild preference for dynamical dark energy and a large value of the Hubble rate param-

eter $H_0 = 74.7_{-4.4}^{+3.4} \text{ km s}^{-1} \text{ Mpc}^{-1}$. A similar approach is adopted in Ref. [33], which combines the sound horizon-independent EFTofLSS analysis of the DESI DR1 galaxy power spectra with the CMB acoustic scale from *Planck* and the uncalibrated BAO measurements from DESI DR1 (which are agnostic to r_s). Finally, let us note that other groups have attempted to directly measure (or forecast the precision of a measurement of) the matter-radiation equality scale to use it as a standard ruler [34–36]. Moreover, another recent method attempt at directly measuring the total energy density (including the baryon-to-matter ratio) from large-scale structure data [37, 38]. We summarize in Fig. 1 the recent sound horizon-free determinations of the Hubble parameter, while we refer to Ref. [39] for a recent review on this topic.

In this paper, we derive updated sound horizon-free cosmological constraints from large-scale structure data, using the power spectrum and bispectrum from BOSS, the 3×2 pt analysis from DES Y3, the C_ℓ^{gg} , $C_\ell^{\kappa g}$ and C_ℓ^{Tg} angular power spectra from the DESI Legacy Imaging Survey DR9, and the CMB gravitational lensing power spectrum from *Planck* PR3. The paper is organised as follows. In Sec. II, we present the sound horizon-free likelihoods considered in this work, while in Sec. III we present our main results. In particular, we first present the constraints from our individual likelihoods, we then discuss the cosmological implications of our combined analysis, before using our analysis as a diagnosis for beyond Λ CDM physics (considering early dark energy and dynamical dark energy cosmologies). We finally conclude in Sec. IV.

II. DATA AND METHOD

A. Datasets

We perform cosmological parameter inference using Markov chain Monte Carlo (MCMC) sampling based on the Metropolis-Hastings algorithm implemented in *MontePython-v3*¹ [40, 41], and interfaced with the Boltzmann solver *CLASS*² [42]. The convergence of our MCMC chains is assessed using the Gelman-Rubin criterion $R - 1 < 0.02$. In our analysis, we consider the following likelihoods:

- **Lensing:** The CMB-marginalized gravitational lensing spectrum from *Planck* 2018 [43].
- **EFTBOSS:** The full-shape analysis of the power spectrum and bispectrum of BOSS luminous red galaxies (LRGs), modeled with the effective field theory of large-scale structure (EFTofLSS) up to

one-loop order.³ The SDSS-III BOSS DR12 galaxy sample is described in Ref. [22]. The power spectrum and bispectrum measurements are taken from Ref. [66], where they were obtained using standard FKP-like estimators [67–74], as implemented in the *Rustico* code⁴ [73, 74]. The covariance matrix, including cross-correlations between the power spectrum and bispectrum, is estimated from 2048 *Patchy* mock catalogs [75], while the survey window function is measured using *fkpwin*⁵ [76]. The measurements are divided into two redshift bins, the CMASS (spanning a redshift range $0.2 < z < 0.43$ with $z_{\text{eff}} = 0.32$) and LOWZ (spanning a redshift range $0.43 < z < 0.7$ with $z_{\text{eff}} = 0.57$) catalogs⁶ [77], that are further split into the north and south galactic skies. The analysis is restricted to mildly nonlinear scales, with $k_{\text{max}} = 0.23 h \text{ Mpc}^{-1}$ for CMASS and $k_{\text{max}} = 0.20 h \text{ Mpc}^{-1}$ for LOWZ. We use an analytically marginalized likelihood [78, 79], adopting Jeffreys priors for the marginalized nuisance parameters to mitigate projection effects [80, 81]. In this paper, we use the *PyBird* likelihood [79], while in App. A we show the excellent agreement between this likelihood and *CLASS-PT* [82, 83], an alternative EFT-based likelihood, in the framework of our sound horizon-free analysis.

- **DESIC $_\ell$:** The auto- and cross- angular power spectra C_ℓ^{gg} , $C_\ell^{\kappa g}$, and C_ℓ^{Tg} likelihood developed in Ref. [84], where g stands for the luminous red galaxies of the DESI Legacy Imaging Survey DR9 [85, 86], κ stands for the *Planck* PR4 Lensing map [87], and T stands for the *Planck* PR4 temperature map [88]. The data are divided into 4 photometric redshift bins ($z_{\text{eff}} = \{0.470, 0.625, 0.785, 0.914\}$) [89, 90], measured by the *NaMaster* code⁷ [91]. The data are analyzed in the linear regime, in the multipole range $20 \leq L \leq 243$, where we do not consider the Limber approximation as in Refs. [89, 90], but use *SwiftC $_\ell$* ⁸ [92], an accurate and differentiable JAX-based code computing the angular galaxy power

¹ https://github.com/brinckmann/montepython_public.

² https://github.com/lesgourg/class_public.

³ The first formulation of the EFTofLSS was carried out in Eulerian space in Refs. [44, 45] and in Lagrangian space in Ref. [46]. Once this theoretical framework was established, many efforts were made to improve this theory and make it predictive, such as the understanding of renormalization [47, 48], the IR-resummation of the long displacement fields [49–54], and the computation of the two-loop matter power spectrum [55, 56]. Then, this theory was developed in the framework of biased tracers (such as galaxies and quasars) in Refs. [57–63], and extended to the bispectrum up to one-loop order in Refs. [64, 65].

⁴ <https://github.com/hectorgil/Rustico>.

⁵ <https://github.com/pierrexyz/fkpwin>.

⁶ <https://data.sdss.org/sas/dr12/boos/lss/>.

⁷ <https://github.com/LSSTDESC/NaMaster>.

⁸ https://cosmo-gitlab.phys.ethz.ch/cosmo_public/swiftcl.

spectrum beyond the Limber approximation using an FFTLog-based method. Our `MontePython-v3` likelihood, inspired from the `MaPar` likelihood⁹ written in `Cobaya` [89, 90], is publicly available here . We refer the reader to Ref. [84] for more details on our likelihood implementation.

- **EFTDES:** The EFTofLSS-based 3×2 pt analysis of DES Y3 data from Ref. [93], which combines galaxy-galaxy clustering, galaxy-galaxy lensing, and cosmic shear [94]. After removing the correlations with the DESI angular power spectrum measurements (see below), the remaining information in the EFTDES likelihood is treated as statistically independent. As done in Ref. [33] (see Sec. 3.5), we do not directly fit the DES data, but we consider Gaussian priors on the key cosmological parameters $\{h, \Omega_m, \sigma_8\}$ coming from the constraints of Ref. [93] (as shown in Tab. 1) to (significantly) accelerate the convergence of our MCMC chains.
- **External Priors:** BBN prior on the baryon density $\omega_b \sim \mathcal{N}(0.02268, 0.00038)$ [95],¹⁰ and a *Planck* prior on the primordial spectral index $n_s \sim \mathcal{N}(0.96, 0.02)$ [1]. In App. A, we instead consider the priors from Ref. [27], namely $\omega_b \sim \mathcal{N}(0.02218, 0.00055)$ and $n_s \sim \mathcal{N}(0.9649, 0.042)$, and show that it does not affect our conclusions.

Our baseline dataset consists of the combination of the above likelihoods. We set uniform wide priors on the parameters $\{\omega_{\text{cdm}}, \ln 10^{10} A_s, h, \alpha_{r_s}\}$, corresponding to the physical dark matter density, the amplitude of the primordial power spectrum, the Hubble parameter $h \equiv H_0/(100 \text{ km/s/Mpc})$, and the BAO location (see below). Concerning the treatment of the neutrino masses, we consider two massless species and one species with $m_\nu = 0.06 \text{ eV}$, following the convention of Ref. [1].

We note that in our analysis we neglect the correlation between EFTBOSS and DESIC_ℓ given that they probe different cosmological volumes [99–101], as well as between EFTBOSS and EFTDES [33]. However, approximately 20% of the DESI Legacy Imaging Surveys footprint overlaps with the DES region used in the EFTDES likelihood [102, 103]. Since most of the constraining power of the DESIC_ℓ likelihood arises from the galaxy auto-spectrum C_ℓ^{gg} , we remeasure this observable to remove the overlapping area with DES and recompute the covariance using `NaMaster` [91]. Given the low signal-to-noise ratio of C_ℓ^{kg} and C_ℓ^{Tg} compared with C_ℓ^{gg} , we further neglect the residual correlation between this observable and EFTDES, which is subdominant. Finally,

when we combine DESIC_ℓ with the CMB lensing likelihood, we remove the overlapping region, namely $\ell < 243$, in the latter likelihood.

B. Method: a sound horizon-free analysis

In this subsection, we explain the extent to which our analysis is independent of information from the sound horizon. First, in order to remove the sound horizon information in the galaxy power spectrum and bispectrum of the EFTBOSS likelihood, we use the wiggle-no-wiggle split method [19, 21, 26, 27]

$$P_{\text{lin}}(k) = P_{\text{nw}}(k) + P_w(\alpha_{r_s} k), \quad (1)$$

marginalizing over the parameter α_{r_s} . We extract the no-wiggle component (*i.e.*, the broadband shape) by Fourier transforming the matter power spectrum into configuration space, then removing the BAO feature and interpolating the broadband shape, before transforming back to Fourier space, following the procedure described in Refs. [82, 104]. Although marginalizing over α_{r_s} removes the oscillatory BAO signal, residual sound horizon information can in principle enter through the baryon suppression scale, β_{r_s} . Ref. [19] shows that, for current LSS surveys, the sound horizon information arising from the broadband shape is negligible.

Second, regarding the CMB gravitational lensing power spectrum, Ref. [24] demonstrated that this observable is an approximately r_s -independent probe, since it is integrated along the line of sight, significantly suppressing the signal from acoustic oscillations.

Third, residual BAO information has also been shown to be negligible in the DESIC_ℓ likelihood. In particular, the DESIC_ℓ analysis of Refs. [105, 106] implements a wiggle–no-wiggle decomposition of the linear matter power spectrum similar to Eq. (1), before performing the projection into the galaxy angular power spectrum. They find that α_{r_s} remains only weakly constrained, confirming the effective sound horizon independence of this probe (see App. B of Ref. [106]).

Finally, regarding the EFTDES analysis [93], it does not allow the BAO angular distance to be determined since (i) the BAO signal lies at larger angular separations, and (ii) the residual BAO signal is smoothed by the projection onto the line of sight (see App. A of Ref. [105]).

III. COSMOLOGICAL RESULTS

A. Internal consistency between the sound horizon-free likelihoods

In the top left panel of Fig. 2, we display the posterior distributions of $\{h, \Omega_m, \sigma_8\}$ obtained from each sound horizon-free likelihood introduced in Sec. II A — namely,

⁹ <https://github.com/NoahSailer/MaPar/tree/main>.

¹⁰ This constraint is based on the theoretical prediction of Ref. [96], the experimental Deuterium fraction of Ref. [97] and the experimental Helium fraction of Ref. [98].

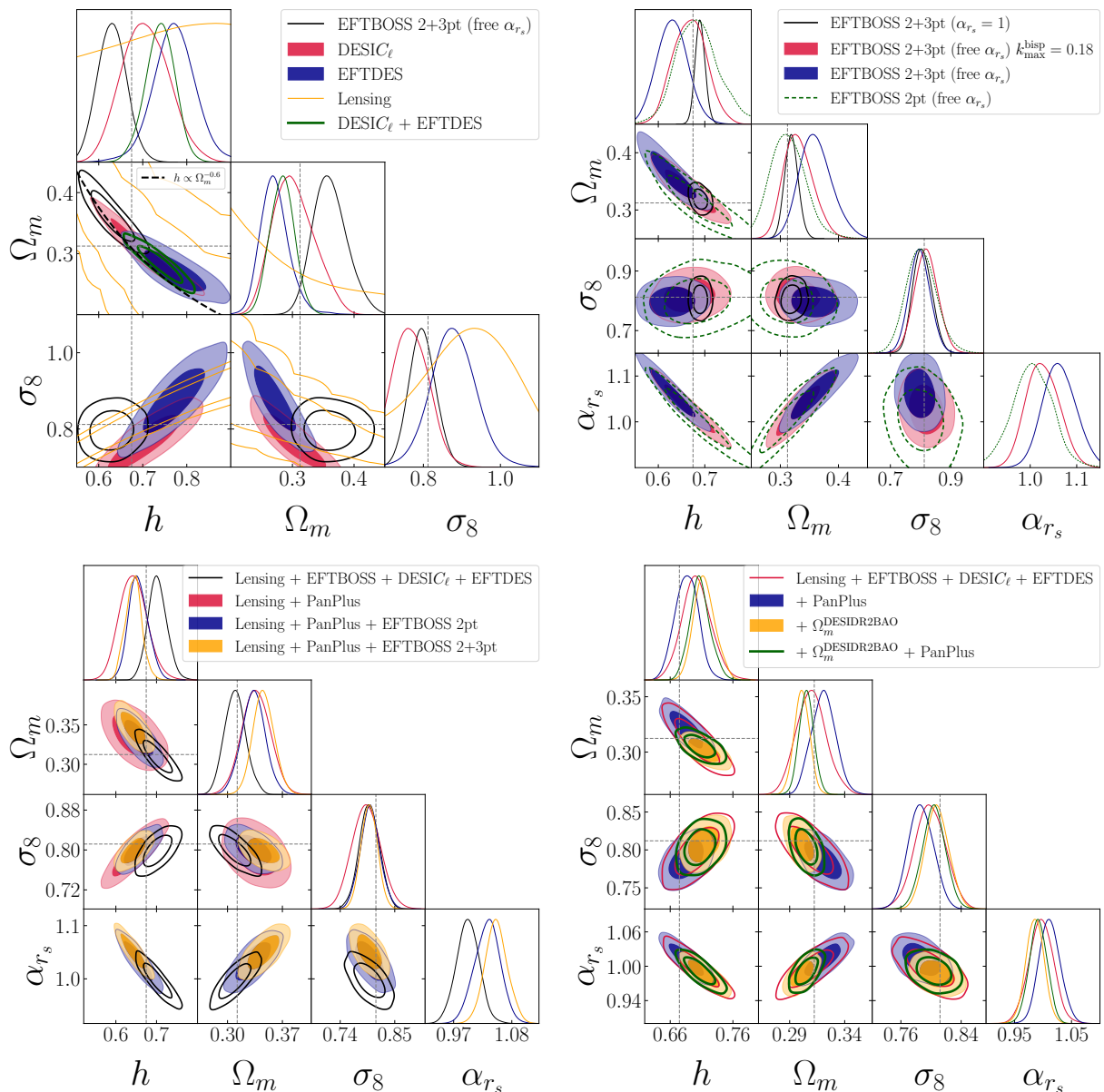


FIG. 2: *Top left* – 2D posterior distributions from the individual sound horizon-free likelihoods considered in this work, with ω_b and n_s fixed. *Top right* – 2D posterior distributions from several EFTBOSS configurations. *Bottom left* – 2D posterior distributions from several sound horizon-free likelihood combinations, using the prior on n_s and ω_b defined in Sec. II A. *Bottom right* – 2D posterior distributions from several combinations between our baseline analysis, Pantheon+ and DESI DR2 BAO. In all panels, the dashed lines correspond to the *Planck* mean values from TTTEEE + Lensing [1].

CMB lensing from *Planck* 2018 (PR3), DESIC_ℓ , EFTDES and EFTBOSS – while in Tab. I we show the associated cosmological constraints. For simplicity, we fix $n_s = 0.965$ [1] and $\omega_b = 0.02235$ [95] in this subsection.

As shown in Fig. 2, CMB lensing alone is not able to constrain h and Ω_m , but it forces the 2D posterior distribution of these parameters to follow the degeneracy direction $h \propto \Omega_m^{-0.6}$ [24]. On the other hand, the DESIC_ℓ , EFTDES and EFTBOSS likelihoods are able

to set significant constraints on those parameters (determined at a $\lesssim 10\%$ precision), while they all follow the CMB lensing degeneracy line in the $\{h, \Omega_m\}$ plane. However, those three likelihoods exhibit different directions in the $\{\Omega_m, \sigma_8\}$ and $\{h, \sigma_8\}$ planes, suggesting that a combination would break these degeneracies. In addition, as shown in Tab. I, we note that EFTBOSS dominates the constraints on h (by $\sim 70\%$ and $\sim 50\%$ compared with DESIC_ℓ and EFTDES), as well as on σ_8 (by

	h	Ω_m	σ_8
DESIC $_\ell$	0.706 ± 0.053	$0.302^{+0.029}_{-0.038}$	0.766 ± 0.048
EFTDES	0.772 ± 0.049	$0.272^{+0.019}_{-0.026}$	0.877 ± 0.059
EFTBOSS	0.630 ± 0.032	$0.361^{+0.025}_{-0.030}$	0.797 ± 0.034
EFTBOSS ($\alpha_{r_s} = 1$)	0.690 ± 0.011	0.319 ± 0.012	$0.806^{+0.030}_{-0.033}$
Lensing + DESIC $_\ell$ + EFTDES + EFTBOSS	$0.702^{+0.022}_{-0.024}$	0.310 ± 0.013	0.799 ± 0.020
Lensing + DESIC $_\ell$ + EFTDES + EFTBOSS + PanPlus	0.686 ± 0.018	0.321 ± 0.011	0.787 ± 0.017
Lensing + DESIC $_\ell$ + EFTDES + EFTBOSS + PanPlus + DESI BAO	$0.708^{+0.015}_{-0.017}$	0.3053 ± 0.0067	0.804 ± 0.015
Lensing + PanPlus + EFTBOSS 2pt	$0.655^{+0.021}_{-0.026}$	0.333 ± 0.015	0.800 ± 0.020
Lensing + PanPlus + EFTBOSS 2+3pt	0.644 ± 0.020	0.346 ± 0.014	0.799 ± 0.017

TABLE I: Cosmological results (posterior mean $\pm 68\%$ CL) from different combinations of sound horizon-free likelihoods.

$\sim 40\%$ and $\sim 70\%$ compared with DESIC $_\ell$ and EFTDES), while EFTDES dominates the constraint on Ω_m by $\sim 40\%$ compared with DESIC $_\ell$ and EFTBOSS. We further note that the DESIC $_\ell$ likelihood is consistent with both the EFTDES (at 1.7σ) and EFTBOSS (at 2.1σ) likelihoods, while the last two likelihoods are slightly inconsistent at 2.6σ , mostly coming from a shift along the $\{h, \Omega_m\}$ degeneracy line.¹¹ Finally, the EFTBOSS, EFTDES and DESIC $_\ell$ likelihoods are consistent with the *Planck* (SHOES [2]) reconstruction of h at 1.4σ (3.0σ), 2.0σ (0.5σ) and 0.6σ (0.8σ), respectively.¹²

B. Internal consistency within the EFTBOSS likelihood

To investigate the internal consistency of the sound horizon-free EFTBOSS likelihood, we first compare, in the top right panel of Fig. 2, the analysis with and without the sound horizon marginalization (“free α_{r_s} ” vs “ $\alpha_{r_s} = 1$ ”). The two analyses are slightly inconsistent, with a 1.8σ shift in h toward lower values and a 1.4σ shift in Ω_m toward higher values. Interestingly, these shifts are accompanied by a deviation of α_{r_s} from unity (or, in other words, from Λ CDM) at 1.8σ , with $\alpha_{r_s} = 1.063^{+0.034}_{-0.038}$. As we discuss in Sec. III D, this behavior may indicate some new physics. This result differs from previous EFTofLSS sound horizon-free studies of BOSS data [20, 21], which include only the power

spectrum, where no deviation was observed between the α_{r_s} -free and α_{r_s} -fix analyses (with $\alpha_{r_s} = 1.011^{+0.036}_{-0.028}$ in Ref. [21] for example),¹³ indicating that the deviation found in our analysis comes from the bispectrum contribution.

Therefore, to quantify the impact of the bispectrum, we compare in the top right panel of Fig. 2 the EFTBOSS sound horizon-free analysis with the power spectrum only (“2pt”), with the one with both the power spectrum and the bispectrum (“2+3pt”). In line with previous studies [20, 21], we report a constraint on α_{r_s} compatible with unity for the 2pt analysis, namely $\alpha_{r_s} = 1.002^{+0.049}_{-0.039}$. Adding the bispectrum, we find an improvement of a factor of ~ 2 in the figure of merit (FoM)¹⁴ of the $\{h, \Omega_m\}$ plane. The small shift between the α_{r_s} -free and the α_{r_s} -fix analyses is caused by the bispectrum contribution, as we observe a 1.0σ shift in h toward lower values and a 1.5σ shift in Ω_m toward higher values when including the bispectrum.

To further investigate the impact of the bispectrum in the sound horizon-free EFTBOSS likelihood, we study in detail the impact of the choice of k_{\max}^B , the maximum bispectrum wavenumber, in both the α_{r_s} -free and α_{r_s} -fix analyses, as shown in Fig. 3. While the constraints on $\{h, \Omega_m, \sigma_8\}$ are quite stable for the α_{r_s} -fix analysis, we observe a shift of $\sim 1.4\sigma$ in h and Ω_m between $k_{\max}^B = 0.18 h \text{ Mpc}^{-1}$ and $k_{\max}^B = 0.20 h \text{ Mpc}^{-1}$ for the α_{r_s} -free analysis.¹⁵ These shifts are accompa-

¹¹ Throughout this work, we quantify the tension between two analyses using the Gaussian tension metric [6, 93] on the $\{h, \Omega_m, \sigma_8\}$ posterior

$$T_N = \sqrt{(\mu_1 - \mu_2)^T (\Sigma_1 + \Sigma_2)^{-1} (\mu_1 - \mu_2)}. \quad (2)$$

¹² We further note that the EFTBOSS, EFTDES and DESIC $_\ell$ likelihoods are consistent with *Planck* (TTTEEE + Lensing) [1] at 1.8σ , 2.2σ and 2.7σ in the $\{h, \Omega_m, \sigma_8\}$ posterior.

¹³ However, we note that Ref. [27] performed a similar analysis with the galaxy power spectra from DESI DR1, and found $q_{\text{BAO}} < 1$ (a parameter analogous to α_{r_s}) at 2σ when combined with *Planck* lensing and Pantheon+. However, this deviation is driven by the discrepancy in Ω_m between Pantheon+ and DESI.

¹⁴ Throughout the paper, in order to quantify an improvement in a 2D posterior distribution of two parameters, we use the ratio of the Figure of Merit (FoM) [14, 107], defined as $\text{FoM} \propto |\det C|^{-1/2}$, where C is the covariance matrix of the parameter posteriors.

¹⁵ We note that our bispectrum analysis includes 170 data points in

nied by an α_{r_s} constraint which becomes $\sim 2\sigma$ away from unity. In addition, as shown in the top right panel of Fig. 2, reducing the maximum bispectrum scale from $k_{\text{max}}^B = 0.23 h \text{ Mpc}^{-1}$ (corresponding to our baseline) to $k_{\text{max}}^B = 0.18 h \text{ Mpc}^{-1}$, mitigates the discrepancy between the α_{r_s} -free and the α_{r_s} -fix analyses from 1.8σ to 0.6σ and restores consistency with $\alpha_{r_s} = 1$. We further note that the inconsistency with EFTDES is reduced from 2.7σ to 1.8σ with $k_{\text{max}}^B = 0.18 h \text{ Mpc}^{-1}$.

C. Combination

The bottom left panel of Fig. 2 presents the constraints from different data combinations of the sound horizon-free likelihoods presented above. Our baseline combination, namely Lensing + EFTBOSS + DESIC $_{\ell}$ + EFTDES, allows to determine the three cosmological parameters $\{h, \Omega_m, \sigma_8\}$ at a 3–4% precision (see Tab. I). Our baseline combination is compatible with *Planck* at 1.2σ , 0.2σ and 0.6σ for h , Ω_m and σ_8 , respectively, while it is consistent with the SH0ES value of h [2] at 2.1σ (see Fig. 1). In addition, our results are compatible with Λ CDM, since we obtain a constraint on α_{r_s} compatible with unity, namely $\alpha_{r_s} = 0.997 \pm 0.022$, and varying the choice of k_{max}^B has only a minor impact on the final reconstructed parameters.

For comparison, we also display, in the bottom left panel of Fig. 2, two previous sound horizon-free analyses, namely Lensing + PanPlus¹⁶ (with a BBN prior on ω_b and a *Planck* prior on n_s), as studied in Ref. [24], as well as Lensing + PanPlus + EFTBOSS 2pt (with free- α_{r_s}), as performed in Refs. [20, 21]. Our baseline analysis improves the $\{h, \Omega_m, \sigma_8\}$ FoM by a factor of ~ 3 compared to the former analysis and by a factor of ~ 1.5 compared to the latter analysis. In addition, to compare with previous α_{r_s} -free BOSS studies, we show in Fig. 2 the impact of the EFTBOSS bispectrum information when added to the Lensing + PanPlus + EFTBOSS 2pt dataset, allowing us to improve the constraints by 15% on h and Ω_m . We further note that while our baseline combination favors a relatively high value of h , the Lensing + PanPlus + EFTBOSS 2pt+3pt combination selects a fairly small value of $h = 0.643 \pm 0.020$ because of the high Ω_m value preferred by Pantheon+. However, we note that across all combinations considered, we recover very consistent constraints on $\sigma_8 \sim 0.799 \pm 0.020$.

The baseline constraints can be further improved by incorporating an external prior on $\Omega_m \sim \mathcal{N}(0.338, 0.018)$ from Pantheon+ (as done in Ref. [21]), as illustrated in

the bottom right panel of Fig. 2. In particular, it tightens the constraints by a factor of ~ 1.5 (in the FoM of $\{h, \Omega_m, \sigma_8\}$) while decreasing the value of h , giving $h = 0.686 \pm 0.018$, reflecting the difference between the preferred matter density in supernova and large-scale structure data [84]. Furthermore, Ref. [33] demonstrated that rescaling the BAO parameters (α_{\parallel} , α_{\perp} , α_{iso}) by α_{r_s} leaves the inferred value of Ω_m from DESI BAO unchanged, implying that this constraint arises entirely from the Alcock-Paczynski effect rather than the sound horizon. Motivated by this result, we also apply a DESI DR2 BAO prior on Ω_m to our baseline dataset, namely $\Omega_m \sim \mathcal{N}(0.2975, 0.0086)$, improving the constraints by a factor of 1.9 and allowing a 2.4% measurement on h free from sound horizon and supernovae data (see the bottom right panel of Fig. 2). Finally, as shown in Fig. 4, we combine the Pantheon+ and DESI DR2 BAO priors on Ω_m with our baseline dataset to obtain the tightest results of our work, namely

$$\begin{aligned} h &= 0.708^{+0.015}_{-0.017}, \\ \Omega_m &= 0.3053 \pm 0.0067, \\ \sigma_8 &= 0.804 \pm 0.015, \end{aligned} \quad (3)$$

corresponding to a 2.3%, 2.2% and 1.9% precision measurements, respectively. Those results are compatible with *Planck* at 1.9σ , 0.7σ and 0.5σ for h , Ω_m and σ_8 , and with SH0ES at 1.3σ for h (see Fig. 1). In Fig. 4, we also display the constraints from our full dataset with α_{r_s} -fix, yielding

$$\begin{aligned} h &= 0.701 \pm 0.010, \\ \Omega_m &= 0.3074 \pm 0.0055, \\ \sigma_8 &= 0.802 \pm 0.015. \end{aligned} \quad (4)$$

The α_{r_s} -free and α_{r_s} -fix analyses are consistent up to 0.4σ on the cosmological parameters, with α_{r_s} compatible with unity ($\alpha_{r_s} = 0.991 \pm 0.016$) in the full analysis.

D. Looking for new physics

It has been shown that the comparison between analyzes that marginalizes over or fix α_{r_s} is a useful diagnosis of the presence of physics beyond Λ CDM in the large-scale structure data. As an example, Ref. [19] considered data from a mock Euclid experiment that were generated to contain the signal from different Early Dark Energy (EDE) [108] models that provide large H_0 . Therein, it is demonstrated that for those mock data, when analyzed under Λ CDM (*i.e.*, ignoring the presence of new physics), a large shift between the inferred value of H_0 can appear between the α_{r_s} -fix and α_{r_s} -free analyses. Such a shift is a signature of a bias induced by using the wrong model to analyze the data.

In order to assess whether the shift we have found in the EFTBOSS likelihood when $k_{\text{max}}^B = 0.23 h \text{ Mpc}^{-1}$ could also entail such a signature, we perform a set of

total. Among them, 99 satisfy $k_1, k_2, k_3 < k_{\text{max}}^B = 0.18 h \text{ Mpc}^{-1}$, while the remaining 71 configurations have at least one side with $k > k_{\text{max}}^B = 0.18 h \text{ Mpc}^{-1}$.

¹⁶ We consider here the Pantheon+ likelihood of uncalibrated luminosity distance of type Ia supernovae (SNeIa) in the range $0.01 < z < 2.3$ [15].

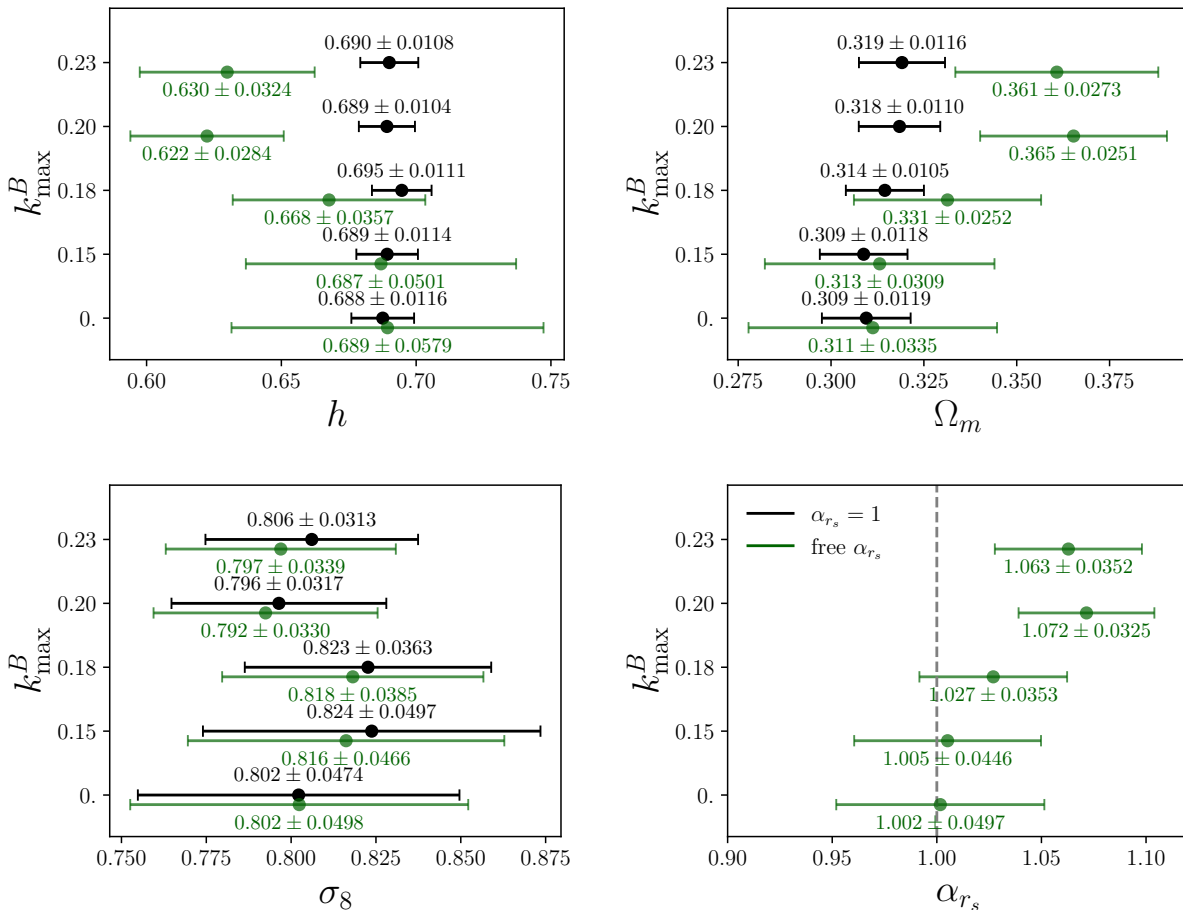


FIG. 3: 1D posterior distributions of $\{h, \Omega_m, \sigma_8, \alpha_{r_s}\}$ from the EFTBOSS 2+3pt analysis for several maximum bispectrum scales k_{max}^B . We display the constraints of the analysis with (in green) and without (in black) the marginalization on the sound horizon.

mock analyses for an EDE cosmology and a dynamical dark energy cosmology [109–116] with parameters specified in Tab. II, chosen to be representative examples from recent analyses. Our results are shown in Fig. 5 for the two different scale cuts we consider in this work, for EDE on the left panel and for w_0w_a on the right panel. We show in green the α_{r_s} -free analyses and in red the α_{r_s} -fix analyses. There are two particularly interesting results coming out of this exercise.

First of all, for the EDE model, we find no differences between the values of h and Ω_m reconstructed in the α_{r_s} -fix or α_{r_s} -free analyses. Moreover, the reconstructed values are compatible with the Λ CDM expectation, despite the mock being generated at values significantly different from Λ CDM. This illustrates the limitation of performing analyses with data of this precision. One cannot conclude that models affecting the sound horizon and leading to large h values are excluded solely based on a Λ CDM analysis: one *expects* to reconstruct low h in that case (see also Ref. [21] for similar results). This conclusion is valid regardless of the value of the scale cut.

Second, for the w_0w_a model, when including information up to $k_{\text{max}}^B = 0.23 h \text{Mpc}^{-1}$, we see a difference of $\sim 1.9\sigma$ between the reconstructed h values, similar in amplitude to what is found with real data ($\sim 2\sigma$), with the α_{r_s} -free analysis being biased low and the α_{r_s} -fix analysis being (slightly) biased high. The difference then reduces to 1σ when the scale cut is restricted to $k_{\text{max}}^B = 0.18 h \text{Mpc}^{-1}$. This result is consistent with Ref. [84] which shows a preference for dynamical dark energy when the bispectrum BOSS data above k_{max}^B are included. This suggests that the behavior we see with real data is reasonable, and is likely another manifestation of the preference for dynamical dark energy observed in the data.

IV. CONCLUSION

In this work, we have carried out a comprehensive sound horizon independent multiprobe cosmological analysis using large-scale structure data from BOSS,

	ω_b	ω_{cdm}	h	$\ln(10^{10} A_s)$	n_s	α_{r_s}	f_{axion}	θ_{scf}	$\log_{10} a_c$	w_0	w_a	Ω_m	σ_8
EDE	0.02253	0.1306	0.7219	3.0978	0.9889	1.0	0.122	2.83	-3.56	-1.0	0.	0.3129	0.8126
DDE	0.02226	0.1187	0.6675	3.0442	0.9700	1.0	-	-	-	-0.7779	-0.7189	0.3177	0.8033

TABLE II: Fiducial cosmological parameters used to generate the mock data. The EDE cosmology is chosen following Ref. [117], while the DDE cosmology is based on the bestfit of Ref. [84].

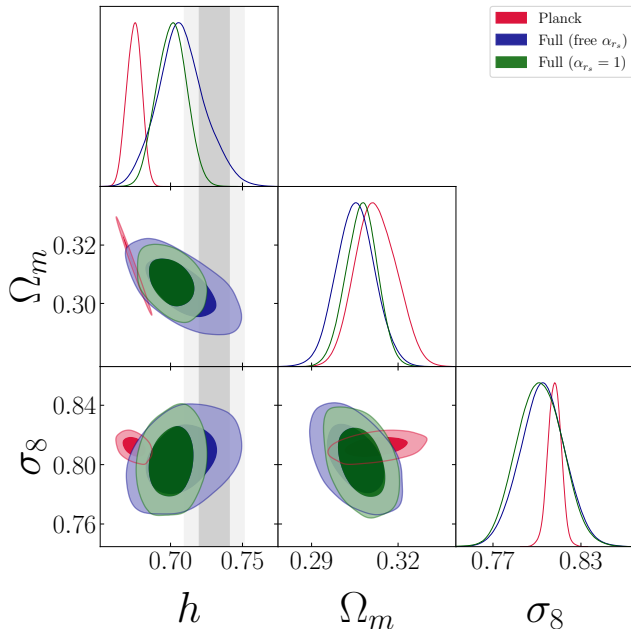


FIG. 4: 2D posterior distributions from the full dataset, namely Lensing + EFTBOSS (2+3pt) + DESIC $_{\ell}$ + EFTDES + PanPlus + $\Omega_m^{\text{DESIDR2BAO}}$, for the α_{r_s} -free and α_{r_s} -fix analyses. For comparison, we display the posteriors from *Planck* [1] in red and the SH0ES constraint on H_0 [2] in grey shaded bands.

DESI, and DES. Our main conclusions can be summarized as follows:

- Individual likelihoods exhibit mild internal tensions up to 2.7σ (between EFTBOSS and EFTDES). The constraints on h and σ_8 are dominated by EFTBOSS, while the constraint on Ω_m is dominated by EFTDES.
- Our EFTBOSS analysis indicates a slight deviation of $\alpha_{r_s} > 1$ at 1.8σ , accompanied by a 1.8σ (1.4σ) shift in h (Ω_m) compared with the analysis that does not marginalize over the sound horizon. This deviation is due to the small scales of the bispectrum $k_{\text{max}}^B > 0.18 h \text{ Mpc}^{-1}$. We further note that including the bispectrum improves the constraint in the $\{h, \Omega_m\}$ plane by a factor of ~ 2 .
- The combination of EFTBOSS, DESIC $_{\ell}$, and EFTDES provides a sufficient statistical power to constrain h , Ω_m , and σ_8 at the 3 – 4% level without

relying on sound horizon information. This represents a significant improvement compared with previous sound horizon-free analyses, namely an improvement by a factor of ~ 3 compared with Lensing + PanPlus [24], and an improvement by a factor of 1.5 compared with Lensing + PanPlus + EFTBOSS 2pt [20, 21]. Our sound horizon independent determination of H_0 lies between the values inferred from CMB and calibrated supernovae measurements, exhibiting a 1.2σ tension with *Planck* and a 2.1σ tension with SH0ES (see Fig. 1).

- We finally perform a Λ CDM fit to EFTBOSS mock data built from an early dark energy (EDE) cosmology and a dynamical dark energy (DDE) cosmology. While for the EDE case, we find no difference in the Λ CDM reconstructed parameters between the sound horizon-free analysis and the full analysis, we find a difference of $\sim 1.9\sigma$ between the reconstructed h values in the DDE case. This indicates that models affecting the sound horizon and leading to large value of h cannot be excluded solely based on a Λ CDM analysis, while we can observe a (slight) inconsistency within the Λ CDM model when fitting to a DDE cosmology. This suggests that the behavior observed with real data is consistent with the recent hint of DDE found when analyzing those data and including information from the sound horizon [84].

The methodology developed in this work is directly applicable to upcoming surveys such as Euclid [118] and LSST [119]. With their larger sky coverage and improved statistical precision, these surveys are expected to deliver significantly tighter sound horizon independent constraints and may help clarify the origin of current cosmological tensions.

ACKNOWLEDGMENTS

We thank Pierre Zhang for valuable suggestions and discussions. ZL acknowledges the hospitality of Tsinghua University and the National Astronomical Observatory of China during the completion of this work. This work was supported in part by the National Key R&D Program of China (2021YFC2203100), by the National Natural Science Foundation of China (12433002, 12261131497), by CAS young interdisciplinary innovation team (JCTD-2022-20), and by 111 Project (B23042).

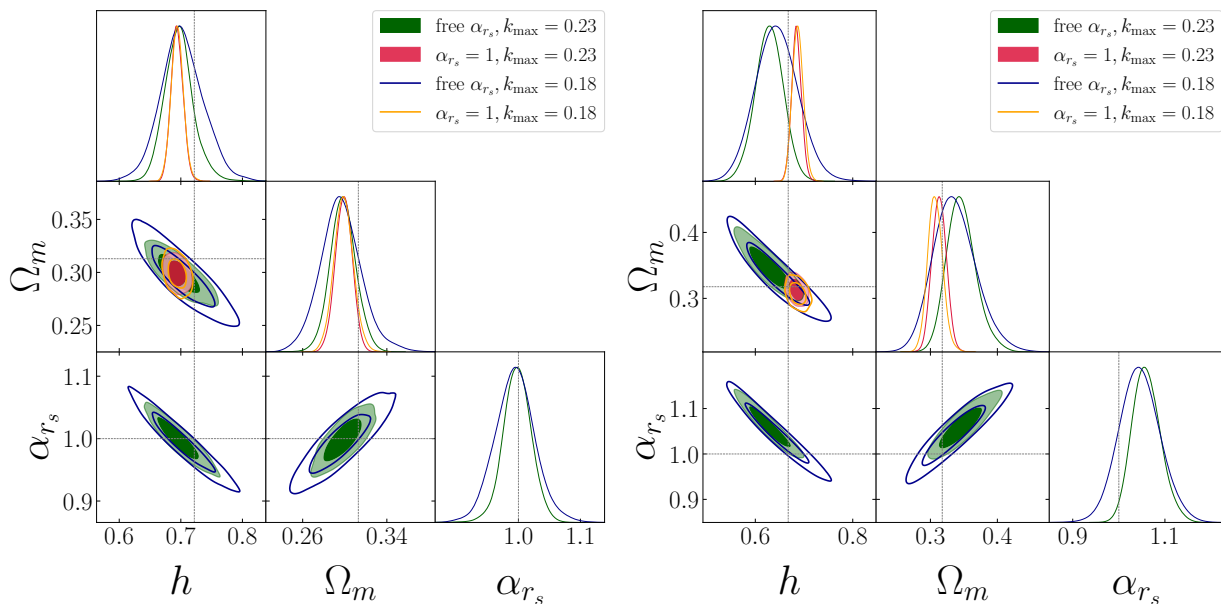


FIG. 5: 2D posterior distributions from the Λ CDM fit to the EFTBOSS 2+3pt mock data generated with the early dark energy cosmology (left panel) and evolving dark energy cosmology (right panel) displayed in Tab. II. The fiducial cosmologies are shown in dashed lines. We show the reconstructed parameters from both the α_{r_s} -free and the α_{r_s} -fix analyses, with the two values of k_{max}^B considered in this work, fixing $n_s = 0.965$ and $\omega_b = 0.02235$.

VP is supported by funding from the European Research Council (ERC) under the European Union’s HORIZON-ERC-2022 (grant agreement no. 101076865). TS and VP acknowledges the European Union’s Horizon Europe research and innovation programme under the Marie Skłodowska-Curie Staff Exchange grant agreement No 101086085 – ASYMMETRY. This work was partially supported by the computational resources from the LUPM’s cloud computing infrastructure founded by Ocevu labex and France-Grilles.

Appendix A: Assessing the robustness of our sound horizon-free analysis

In this appendix, we investigate the impact of (i) the choice of priors on the cosmological parameters ω_b and n_s , and (ii) the EFT likelihood used for the EFTBOSS analysis.

First, we test whether changing the priors from $\omega_b \sim \mathcal{N}(0.02268, 0.00038)$ and $n_s \sim \mathcal{N}(0.96, 0.02)$ included in our baseline analysis to $\omega_b \sim \mathcal{N}(0.02218, 0.00055)$ and

$n_s \sim \mathcal{N}(0.9649, 0.042)$, following Ref. [27], can affect our cosmological constraints. The left panel of Fig. 6 shows that the resulting changes in the posterior distributions are negligible, namely $\lesssim 0.3\sigma$. This indicates that our results are largely insensitive to the ω_b prior, confirming that our analysis remains effectively independent of information from the sound horizon.

Second, we cross-check our sound horizon-free EFTBOSS analysis, obtained with Pybird [79] (using the West-Coast basis [78, 120]), against an independent pipeline, CLASS-PT [82, 83] (using the East-Coast basis [59, 121]). While previous works, such as [122–124], compared these two codes when α_{r_s} is fixed, we compare here the consistency between Pybird and CLASS-PT for an α_{r_s} -free analysis using the galaxy power spectrum (2pt) in the right panel of Fig. 6. Despite differences in EFT basis conventions and numerical implementations between the two codes (see details in Ref. [123]) leading to results that differ at the 1σ level on the Λ CDM parameters (in particular on A_s , σ_8 and Ω_m) for an α_{r_s} -fix analysis [123–126], we find here an excellent agreement at $\lesssim 0.5\sigma$ for the α_{r_s} -free analysis.

-
- [1] N. Aghanim *et al.* (Planck), *Astron. Astrophys.* **641**, A6 (2020), [Erratum: *Astron. Astrophys.* 652, C4 (2021)], arXiv:1807.06209 [astro-ph.CO].
- [2] A. G. Riess *et al.*, *Astrophys. J. Lett.* **934**, L7 (2022), arXiv:2112.04510 [astro-ph.CO].
- [3] S. Casertano *et al.* (H0DN), (2025), arXiv:2510.23823

- [astro-ph.CO].
- [4] T. Louis *et al.* (Atacama Cosmology Telescope), *JCAP* **11**, 062 (2025), arXiv:2503.14452 [astro-ph.CO].
- [5] E. Camphuis *et al.* (SPT-3G), (2025), arXiv:2506.20707 [astro-ph.CO].
- [6] M. Abdul Karim *et al.* (DESI), *Phys. Rev. D* **112**,

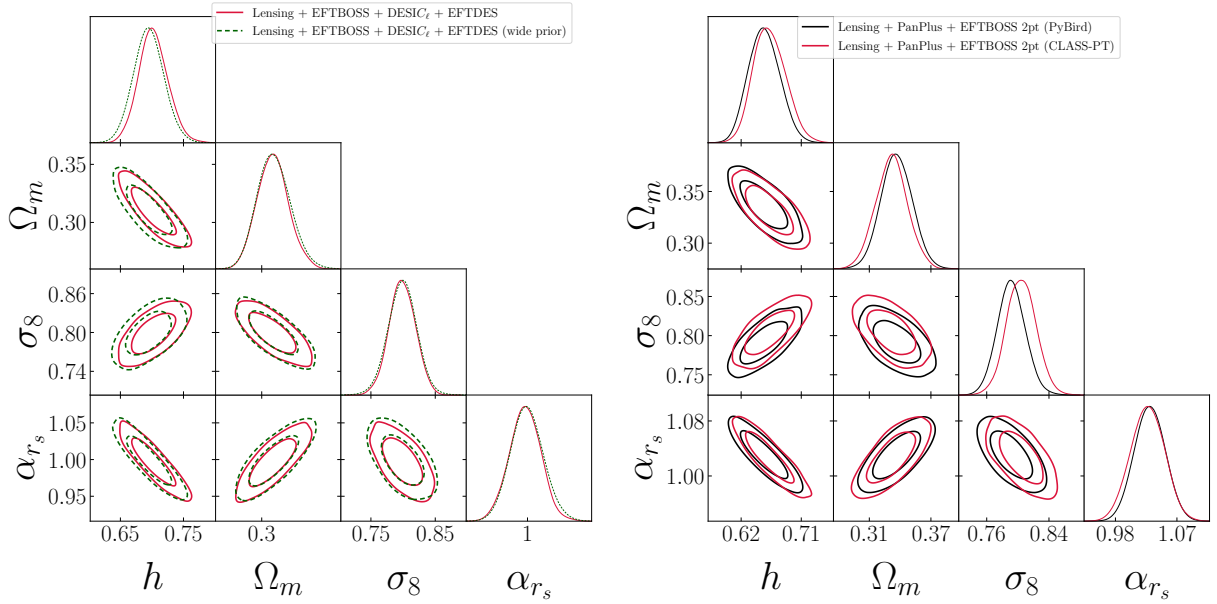


FIG. 6: *Left*: 2D posterior distributions from our baseline analysis, using the ω_b and n_s priors specified in Sec. II A [$\omega_b \sim \mathcal{N}(0.02268, 0.00038)$ and $n_s \sim \mathcal{N}(0.96, 0.02)$], and the same analysis considering different (and wider) priors on these parameters [$\omega_b \sim \mathcal{N}(0.02218, 0.00055)$ and $n_s \sim \mathcal{N}(0.9649, 0.042)$]. *Right*: 2D posterior distributions from the galaxy power spectrum α_{r_s} -free EFTBOSS analysis (combined with Lensing + PanPlus) obtained either with PyBird or CLASS-PT.

- 083515 (2025), arXiv:2503.14738 [astro-ph.CO].
- [7] T. M. C. Abbott *et al.* (DES), (2026), arXiv:2601.14559 [astro-ph.CO].
- [8] T. M. C. Abbott *et al.* (Kilo-Degree Survey, DES), *Open J. Astrophys.* **6**, 2305.17173 (2023), arXiv:2305.17173 [astro-ph.CO].
- [9] M. Asgari *et al.* (KiDS), *Astron. Astrophys.* **645**, A104 (2021), arXiv:2007.15633 [astro-ph.CO].
- [10] I. Pantos and L. Perivolaropoulos, (2026), arXiv:2602.12238 [astro-ph.CO].
- [11] A. H. Wright *et al.*, *Astron. Astrophys.* **703**, A158 (2025), arXiv:2503.19441 [astro-ph.CO].
- [12] T. Simon, P. Zhang, and V. Poulin, *JCAP* **07**, 041 (2023), arXiv:2210.14931 [astro-ph.CO].
- [13] R. Neveux *et al.* (eBOSS), *Mon. Not. Roy. Astron. Soc.* **499**, 210 (2020), arXiv:2007.08999 [astro-ph.CO].
- [14] A. G. Adame *et al.* (DESI), *JCAP* **07**, 028 (2025), arXiv:2411.12022 [astro-ph.CO].
- [15] D. Brout *et al.*, *Astrophys. J.* **938**, 110 (2022), arXiv:2202.04077 [astro-ph.CO].
- [16] D. Rubin *et al.*, *Astrophys. J.* **986**, 231 (2025), arXiv:2311.12098 [astro-ph.CO].
- [17] T. M. C. Abbott *et al.* (DES), *Astrophys. J. Lett.* **973**, L14 (2024), arXiv:2401.02929 [astro-ph.CO].
- [18] B. Popovic *et al.* (DES), (2025), arXiv:2511.07517 [astro-ph.CO].
- [19] G. S. Farren, O. H. E. Philcox, and B. D. Sherwin, *Phys. Rev. D* **105**, 063503 (2022), arXiv:2112.10749 [astro-ph.CO].
- [20] O. H. E. Philcox, G. S. Farren, B. D. Sherwin, E. J. Baxter, and D. J. Brout, *Phys. Rev. D* **106**, 063530 (2022), arXiv:2204.02984 [astro-ph.CO].
- [21] T. L. Smith, V. Poulin, and T. Simon, *Phys. Rev. D* **108**, 103525 (2023), arXiv:2208.12992 [astro-ph.CO].
- [22] S. Alam *et al.* (BOSS), *Mon. Not. Roy. Astron. Soc.* **470**, 2617 (2017), arXiv:1607.03155 [astro-ph.CO].
- [23] V. Poulin, T. L. Smith, R. Calderón, and T. Simon, *Phys. Rev. D* **111**, 083552 (2025), arXiv:2407.18292 [astro-ph.CO].
- [24] E. J. Baxter and B. D. Sherwin, *Mon. Not. Roy. Astron. Soc.* **501**, 1823 (2021), arXiv:2007.04007 [astro-ph.CO].
- [25] O. H. E. Philcox, B. D. Sherwin, G. S. Farren, and E. J. Baxter, *Phys. Rev. D* **103**, 023538 (2021), arXiv:2008.08084 [astro-ph.CO].
- [26] K. Ghaemi, N. Schöneberg, and L. Verde, *JCAP* **11**, 029 (2025), arXiv:2504.10578 [astro-ph.CO].
- [27] E. A. Zaborowski *et al.*, *JCAP* **06**, 020 (2025), arXiv:2411.16677 [astro-ph.CO].
- [28] S. Brieden, H. Gil-Marín, and L. Verde, *JCAP* **12**, 054 (2021), arXiv:2106.07641 [astro-ph.CO].
- [29] S. Brieden, H. Gil-Marín, and L. Verde, *JCAP* **04**, 023 (2023), arXiv:2212.04522 [astro-ph.CO].
- [30] L. Pogosian, G.-B. Zhao, and K. Jedamzik, *Astrophys. J. Lett.* **904**, L17 (2020), arXiv:2009.08455 [astro-ph.CO].
- [31] H. García Escudero, S. H. Mirpoorian, and L. Pogosian, *Astrophys. J. Lett.* **998**, L41 (2026), arXiv:2509.16202 [astro-ph.CO].
- [32] R. K. Sharma and J. Lesgourgues, (2025), arXiv:2510.15835 [astro-ph.CO].
- [33] E. A. Zaborowski *et al.*, (2025), arXiv:2510.19149 [astro-ph.CO].
- [34] S. Cunnington, *Mon. Not. Roy. Astron. Soc.* **512**, 2408 (2022), arXiv:2202.13828 [astro-ph.CO].
- [35] Y. Lai, C. Howlett, and T. Davis, *JCAP* **10**, 071 (2025), arXiv:2507.11823 [astro-ph.CO].

- [36] B. Bahr-Kalus, D. Parkinson, and E.-M. Mueller, *Mon. Not. Roy. Astron. Soc.* **524**, 2463 (2023), [Erratum: *Mon. Not. Roy. Astron. Soc.* 526, 3248–3249 (2023)], arXiv:2302.07484 [astro-ph.CO].
- [37] A. Krolewski, W. J. Percival, and A. Woodfinden, (2024), arXiv:2403.19227 [astro-ph.CO].
- [38] A. Krolewski and W. J. Percival, (2024), arXiv:2403.19236 [astro-ph.CO].
- [39] I. Pantos and L. Perivolaropoulos, (2026), arXiv:2601.00650 [astro-ph.CO].
- [40] B. Audren, J. Lesgourgues, K. Benabed, and S. Prunet, *JCAP* **1302**, 001 (2013), arXiv:1210.7183 [astro-ph.CO].
- [41] T. Brinckmann and J. Lesgourgues, “MontePython 3: boosted MCMC sampler and other features,” (2018), arXiv:1804.07261 [astro-ph.CO].
- [42] D. Blas, J. Lesgourgues, and T. Tram, *JCAP* **07**, 034 (2011), arXiv:1104.2933 [astro-ph.CO].
- [43] N. Aghanim *et al.* (Planck), *Astron. Astrophys.* **641**, A8 (2020), arXiv:1807.06210 [astro-ph.CO].
- [44] J. J. M. Carrasco, M. P. Hertzberg, and L. Senatore, *JHEP* **09**, 082 (2012), arXiv:1206.2926 [astro-ph.CO].
- [45] D. Baumann, A. Nicolis, L. Senatore, and M. Zaldarriaga, *JCAP* **07**, 051 (2012), arXiv:1004.2488 [astro-ph.CO].
- [46] R. A. Porto, L. Senatore, and M. Zaldarriaga, *JCAP* **05**, 022 (2014), arXiv:1311.2168 [astro-ph.CO].
- [47] E. Pajer and M. Zaldarriaga, *JCAP* **08**, 037 (2013), arXiv:1301.7182 [astro-ph.CO].
- [48] A. A. Abolhasani, M. Mirbabayi, and E. Pajer, *JCAP* **05**, 063 (2016), arXiv:1509.07886 [hep-th].
- [49] L. Senatore and M. Zaldarriaga, (2014), arXiv:1409.1225 [astro-ph.CO].
- [50] T. Baldauf, M. Mirbabayi, M. Simonović, and M. Zaldarriaga, *Phys. Rev. D* **92**, 043514 (2015), arXiv:1504.04366 [astro-ph.CO].
- [51] L. Senatore and M. Zaldarriaga, *JCAP* **02**, 013 (2015), arXiv:1404.5954 [astro-ph.CO].
- [52] L. Senatore and G. Trevisan, *JCAP* **05**, 019 (2018), arXiv:1710.02178 [astro-ph.CO].
- [53] M. Lewandowski and L. Senatore, *JCAP* **03**, 018 (2020), arXiv:1810.11855 [astro-ph.CO].
- [54] D. Blas, M. Garny, M. M. Ivanov, and S. Sibiryakov, *JCAP* **07**, 028 (2016), arXiv:1605.02149 [astro-ph.CO].
- [55] J. J. M. Carrasco, S. Foreman, D. Green, and L. Senatore, *JCAP* **07**, 056 (2014), arXiv:1304.4946 [astro-ph.CO].
- [56] J. J. M. Carrasco, S. Foreman, D. Green, and L. Senatore, *JCAP* **07**, 057 (2014), arXiv:1310.0464 [astro-ph.CO].
- [57] P. McDonald and A. Roy, *JCAP* **08**, 020 (2009), arXiv:0902.0991 [astro-ph.CO].
- [58] L. Senatore, *JCAP* **11**, 007 (2015), arXiv:1406.7843 [astro-ph.CO].
- [59] M. Mirbabayi, F. Schmidt, and M. Zaldarriaga, *JCAP* **07**, 030 (2015), arXiv:1412.5169 [astro-ph.CO].
- [60] R. Angulo, M. Fasiello, L. Senatore, and Z. Vlah, *JCAP* **09**, 029 (2015), arXiv:1503.08826 [astro-ph.CO].
- [61] T. Fujita, V. Mauerhofer, L. Senatore, Z. Vlah, and R. Angulo, *JCAP* **01**, 009 (2020), arXiv:1609.00717 [astro-ph.CO].
- [62] A. Perko, L. Senatore, E. Jennings, and R. H. Wechsler, (2016), arXiv:1610.09321 [astro-ph.CO].
- [63] E. O. Nadler, A. Perko, and L. Senatore, *JCAP* **02**, 058 (2018), arXiv:1710.10308 [astro-ph.CO].
- [64] G. D’Amico, Y. Donath, M. Lewandowski, L. Senatore, and P. Zhang, *JCAP* **07**, 041 (2024), arXiv:2211.17130 [astro-ph.CO].
- [65] O. H. E. Philcox, M. M. Ivanov, G. Cabass, M. Simonović, M. Zaldarriaga, and T. Nishimichi, *Phys. Rev. D* **106**, 043530 (2022), arXiv:2206.02800 [astro-ph.CO].
- [66] G. D’Amico, Y. Donath, M. Lewandowski, L. Senatore, and P. Zhang, *JCAP* **05**, 059 (2024), arXiv:2206.08327 [astro-ph.CO].
- [67] H. A. Feldman, N. Kaiser, and J. A. Peacock, *Astrophys. J.* **426**, 23 (1994), arXiv:astro-ph/9304022.
- [68] K. Yamamoto, M. Nakamichi, A. Kamino, B. A. Bassett, and H. Nishioka, *Publ. Astron. Soc. Jap.* **58**, 93 (2006), arXiv:astro-ph/0505115.
- [69] N. Hand, Y. Li, Z. Slepian, and U. Seljak, *JCAP* **07**, 002 (2017), arXiv:1704.02357 [astro-ph.CO].
- [70] D. Bianchi, H. Gil-Marín, R. Ruggeri, and W. J. Percival, *Mon. Not. Roy. Astron. Soc.* **453**, L11 (2015), arXiv:1505.05341 [astro-ph.CO].
- [71] F. Beutler *et al.* (BOSS), *Mon. Not. Roy. Astron. Soc.* **443**, 1065 (2014), arXiv:1312.4611 [astro-ph.CO].
- [72] R. Scoccimarro, *Phys. Rev. D* **92**, 083532 (2015), arXiv:1506.02729 [astro-ph.CO].
- [73] H. Gil-Marín *et al.* (BOSS), *Mon. Not. Roy. Astron. Soc.* **460**, 4188 (2016), arXiv:1509.06386 [astro-ph.CO].
- [74] H. Gil-Marín, W. J. Percival, L. Verde, J. R. Brownstein, C.-H. Chuang, F.-S. Kitaura, S. A. Rodríguez-Torres, and M. D. Olmstead, *Mon. Not. Roy. Astron. Soc.* **465**, 1757 (2017), arXiv:1606.00439 [astro-ph.CO].
- [75] F.-S. Kitaura *et al.*, *Mon. Not. Roy. Astron. Soc.* **456**, 4156 (2016), arXiv:1509.06400 [astro-ph.CO].
- [76] F. Beutler, E. Castorina, and P. Zhang, *JCAP* **03**, 040 (2019), arXiv:1810.05051 [astro-ph.CO].
- [77] B. Reid *et al.* (BOSS), *Mon. Not. Roy. Astron. Soc.* **455**, 1553 (2016), arXiv:1509.06529 [astro-ph.CO].
- [78] G. D’Amico, J. Gleyzes, N. Kokron, K. Markovic, L. Senatore, P. Zhang, F. Beutler, and H. Gil-Marín, *JCAP* **05**, 005 (2020), arXiv:1909.05271 [astro-ph.CO].
- [79] G. D’Amico, L. Senatore, and P. Zhang, *JCAP* **01**, 006 (2021), arXiv:2003.07956 [astro-ph.CO].
- [80] A. Reeves, P. Zhang, and H. Zheng, (2025), arXiv:2507.20991 [astro-ph.CO].
- [81] B. Hadzhiyska, K. Wolz, S. Azzoni, D. Alonso, C. García-García, J. Ruiz-Zapatero, and A. Slosar, (2023), 10.21105/astro.2301.11895, arXiv:2301.11895 [astro-ph.CO].
- [82] A. Chudaykin, M. M. Ivanov, O. H. E. Philcox, and M. Simonović, *Phys. Rev. D* **102**, 063533 (2020), arXiv:2004.10607 [astro-ph.CO].
- [83] O. H. E. Philcox and M. M. Ivanov, *Phys. Rev. D* **105**, 043517 (2022), arXiv:2112.04515 [astro-ph.CO].
- [84] Z. Lu and T. Simon, (2025), arXiv:2511.10616 [astro-ph.CO].
- [85] R. Zhou *et al.*, *JCAP* **11**, 097 (2023), arXiv:2309.06443 [astro-ph.CO].
- [86] R. Zhou *et al.* (DESI), *Astron. J.* **165**, 58 (2023), arXiv:2208.08515 [astro-ph.CO].
- [87] J. Carron, M. Mirmelstein, and A. Lewis, *JCAP* **09**, 039 (2022), arXiv:2206.07773 [astro-ph.CO].
- [88] Y. Akrami *et al.* (Planck), *Astron. Astrophys.* **643**, A42 (2020), arXiv:2007.04997 [astro-ph.CO].
- [89] N. Sailer *et al.*, *JCAP* **06**, 008 (2025), arXiv:2407.04607 [astro-ph.CO].

- [90] J. Kim *et al.*, *JCAP* **12**, 022 (2024), arXiv:2407.04606 [astro-ph.CO].
- [91] D. Alonso, J. Sanchez, and A. Slosar (LSST Dark Energy Science), *Mon. Not. Roy. Astron. Soc.* **484**, 4127 (2019), arXiv:1809.09603 [astro-ph.CO].
- [92] L. Reymond, A. Reeves, P. Zhang, and A. Refregier, (2025), arXiv:2505.22718 [astro-ph.CO].
- [93] G. D’Amico, A. Refregier, L. Senatore, and P. Zhang, (2025), arXiv:2510.24878 [astro-ph.CO].
- [94] T. Abbott *et al.* (DES), *Mon. Not. Roy. Astron. Soc.* **460**, 1270 (2016), arXiv:1601.00329 [astro-ph.CO].
- [95] N. Schöneberg, J. Lesgourgues, and D. C. Hooper, *JCAP* **10**, 029 (2019), arXiv:1907.11594 [astro-ph.CO].
- [96] R. Consiglio, P. F. de Salas, G. Mangano, G. Miele, S. Pastor, and O. Pisanti, *Comput. Phys. Commun.* **233**, 237 (2018), arXiv:1712.04378 [astro-ph.CO].
- [97] R. J. Cooke, M. Pettini, and C. C. Steidel, *Astrophys. J.* **855**, 102 (2018), arXiv:1710.11129 [astro-ph.CO].
- [98] E. Aver, K. A. Olive, and E. D. Skillman, *JCAP* **07**, 011 (2015), arXiv:1503.08146 [astro-ph.CO].
- [99] P. L. Taylor and K. Markovič, *Phys. Rev. D* **106**, 063536 (2022), arXiv:2205.14167 [astro-ph.CO].
- [100] M. Maus *et al.*, *JCAP* **11**, 077 (2025), arXiv:2505.20656 [astro-ph.CO].
- [101] M. M. Ivanov, J. M. Sullivan, S.-F. Chen, A. Chudaykin, M. Maus, and O. H. E. Philcox, (2026), arXiv:2601.16165 [astro-ph.CO].
- [102] A. Dey *et al.* (DESI), *Astron. J.* **157**, 168 (2019), arXiv:1804.08657 [astro-ph.IM].
- [103] T. M. C. Abbott *et al.* (DES), *Phys. Rev. D* **105**, 023520 (2022), arXiv:2105.13549 [astro-ph.CO].
- [104] J. Hamann, S. Hannestad, J. Lesgourgues, C. Rampf, and Y. Y. Y. Wong, *JCAP* **07**, 022 (2010), arXiv:1003.3999 [astro-ph.CO].
- [105] A. Reeves, A. Nicola, and A. Refregier, *JCAP* **06**, 042 (2025), arXiv:2502.01722 [astro-ph.CO].
- [106] A. Reeves, S. Ferraro, A. Nicola, and A. Refregier, (2025), arXiv:2510.06114 [astro-ph.CO].
- [107] A. Albrecht *et al.*, (2006), arXiv:astro-ph/0609591.
- [108] V. Poulin, T. L. Smith, T. Karwal, and M. Kamionkowski, *Phys. Rev. Lett.* **122**, 221301 (2019), arXiv:1811.04083 [astro-ph.CO].
- [109] Y. Cai, X. Ren, T. Qiu, M. Li, and X. Zhang, (2025), arXiv:2505.24732 [astro-ph.CO].
- [110] Y.-F. Cai, E. N. Saridakis, M. R. Setare, and J.-Q. Xia, *Phys. Rept.* **493**, 1 (2010), arXiv:0909.2776 [hep-th].
- [111] B. Feng, X.-L. Wang, and X.-M. Zhang, *Phys. Lett. B* **607**, 35 (2005), arXiv:astro-ph/0404224.
- [112] J.-Q. Xia, Y.-F. Cai, T.-T. Qiu, G.-B. Zhao, and X. Zhang, *Int. J. Mod. Phys. D* **17**, 1229 (2008), arXiv:astro-ph/0703202.
- [113] G.-B. Zhao, R. G. Crittenden, L. Pogosian, and X. Zhang, *Phys. Rev. Lett.* **109**, 171301 (2012), arXiv:1207.3804 [astro-ph.CO].
- [114] Z.-K. Guo, Y.-S. Piao, X.-M. Zhang, and Y.-Z. Zhang, *Phys. Lett. B* **608**, 177 (2005), arXiv:astro-ph/0410654.
- [115] G.-B. Zhao, J.-Q. Xia, M. Li, B. Feng, and X. Zhang, *Phys. Rev. D* **72**, 123515 (2005), arXiv:astro-ph/0507482.
- [116] J.-Q. Xia, G.-B. Zhao, B. Feng, H. Li, and X. Zhang, *Phys. Rev. D* **73**, 063521 (2006), arXiv:astro-ph/0511625.
- [117] T. L. Smith, V. Poulin, and M. A. Amin, *Phys. Rev. D* **101**, 063523 (2020), arXiv:1908.06995 [astro-ph.CO].
- [118] R. Laureijs *et al.* (EUCLID), (2011), arXiv:1110.3193 [astro-ph.CO].
- [119] Ž. Ivezić *et al.* (LSST), *Astrophys. J.* **873**, 111 (2019), arXiv:0805.2366 [astro-ph].
- [120] G. D’Amico, Y. Donath, L. Senatore, and P. Zhang, *JCAP* **03**, 032 (2024), arXiv:2012.07554 [astro-ph.CO].
- [121] T. Fujita and Z. Vlah, *JCAP* **10**, 059 (2020), arXiv:2003.10114 [astro-ph.CO].
- [122] T. Nishimichi, G. D’Amico, M. M. Ivanov, L. Senatore, M. Simonović, M. Takada, M. Zaldarriaga, and P. Zhang, *Phys. Rev. D* **102**, 123541 (2020), arXiv:2003.08277 [astro-ph.CO].
- [123] T. Simon, P. Zhang, V. Poulin, and T. L. Smith, *Phys. Rev. D* **107**, 123530 (2023), arXiv:2208.05929 [astro-ph.CO].
- [124] E. B. Holm, L. Herold, T. Simon, E. G. M. Ferreira, S. Hannestad, V. Poulin, and T. Tram, *Phys. Rev. D* **108**, 123514 (2023), arXiv:2309.04468 [astro-ph.CO].
- [125] P. Carrilho, C. Moretti, and A. Pourtsidou, *JCAP* **01**, 028 (2023), arXiv:2207.14784 [astro-ph.CO].
- [126] R. Gspaner, R. Zhao, J. Donald-McCann, D. Bacon, K. Koyama, R. Crittenden, T. Simon, and E.-M. Mueller, *Mon. Not. Roy. Astron. Soc.* **530**, 3075 (2024), arXiv:2312.01977 [astro-ph.CO].